Bioorganic & Medicinal Chemistry 21 (2013) 6239–6246

Contents lists available at SciVerse ScienceDirect

Bioorganic & Medicinal Chemistry

journal homepage: www.elsevier.com/locate/bmc

RNA-aptamers that modulate the RhoGEF activity of Tiam1

Björn Niebel [†], Christine I. Wosnitza [†], Michael Famulok [*]

Life and Medical Sciences (LIMES) Institute, University of Bonn, Gerhard-Domagk-Str 1, 53121 Bonn, Germany

ARTICLE INFO

Article history:
Available online 23 May 2013

Keywords:
In vitro selection
Tiaml
Anti-RhoGEF aptamer
SELEX
RNA aptamers

ABSTRACT

Rho GTPases regulate the actin cytoskeleton and thereby control cell migration, cell morphology, cell motility, and other cellular functions. The gene product of the oncogene Tiam1 acts as a guanine nucleotide exchange factor (GEF) for the Rho GTPase Rac. Like other RhoGEFs, Tiam1 is involved in cancer progression, but it also counteracts invasion in different cancer cell types. Hence, further investigations are required to unravel the functions of Tiam1 in the context of cancer initiation and progression, which appear to be cell specific. Although RhoGEFs in general seem to be attractive therapeutic targets, not many inhibitors have been described, yet. Here we report the identification and characterization of inhibitory RNA aptamers that specifically target Tiam1. After 16 selection rounds three aptamers sharing a 15 nucleotides consensus motif were identified. The clones K91 and K11 inhibited the Tiam1-mediated activation of the GTPase Rac2 in vitro. The tightest binder K91 neither bound the Rho GEF Vav1 nor the Arf GEF Cytohesin-2. In the presence of Rac1, the binding of K91 to Tiam1 was impaired indicating that the binding motif on Tiam1 overlaps with the GTPase binding site. K91 and K11 are the first reported inhibitory molecules targeting the GEF function of Tiam1. Due to their specificity over related GEF proteins they may represent promising tools for further elucidation of the biological functions of Tiam1. We anticipated that these aptamers will prove useful in validating the ambiguous roles of Tiam1 in cancer biology.

1. Introduction

Proteins of the Ras superfamily of small GTPases play pivotal roles in signal transduction. They bind and hydrolyze GTP and thus cycle between an active (GTP) and an inactive (GDP) state. Their nucleotide binding state is usually regulated by GTPase activating proteins (GAPs) that accelerate the hydrolysis activity, and by guanine nucleotide exchange factors (GEFs), which catalyze the intrinsically slow nucleotide exchange from GDP to GTP and thereby activate the GTPase.[1] One branch of the Ras superfamily of small GTPases is represented by Rho GTPases that are well characterized for their ability to regulate cell migration, cell morphology, cell motility, and the organization of the actin cytoskeleton.[2,3] In addition, Rho GTPases are involved in a variety of cancer types.[4] The distinct mammalian RhoGEF proteins comprise Dbl-homology (DH) and Dedicator of cytokinesis (DOCK) domains. With currently 68 members DH domain containing GEF proteins represent the largest group.[1] Dbl, the eponym of the DH domain, was originally identified as an oncogene in a human B-cell lymphoma.[5] Ever since there have been found a lot more Dbl-like members as proto-oncogenes, for example *vav*, *lfc*, *lbc*, *tim*, *ost*, *net1*, or *dbs*.[6–12] Among them, Tiam1 has been identified as a T-lymphoma invasive and metastasis inducing protein and was named accordingly.[13] Besides the DH domain (amino acids 1040–1234; see Fig. 1A) that exclusively activates Rho GTPases,[14,15] Tiam1 further consists of an N-terminal PH-CC-Ex module (amino acids 434–702; see Fig. 1A) that allows the protein to interact with poly-phosphorylated phospholipids at the plasma membrane. The neighboring Ras binding domain that ranges from residue 765 to 832 (RBD, Fig. 1A) enables Tiam1 to interact with the active form of Ras and thus connects Tiam1 signaling events with the Ras pathway.[16] There is increasing evidence that Tiam1 expression directly correlates with the grade of human gastric cancer, prostate carcinoma and murine colon carcinoma.[17–19] Conversely, depending on the cell type, Tiam1 is also capable of inhibiting invasion in epithelial cells and in metastatic melanoma cells.[20,21] On this account much more effort is required to unravel the cell-specific functions of Tiam1 in the context of cancer initiation and progression.

However, even though RhoGEFs seem to be attractive therapeutic targets, the number of molecular tools that has been described for the selective modulation of this protein family is scarce. Only one small molecule inhibitor for the N-terminal DH domain of Trio[22,23] and a peptide aptamer targeting TrioGEFD2 have been reported to date.[24] A variant of the peptide aptamer was further developed to specifically target the oncogenic isoform of the Rho-GEF word division Trio (Tgat).[25] Therefore, targeting of this protein class with conventional small molecule-based inhibitors appears to be rather difficult. To address this issue, we sought to

* Corresponding author. Tel.: +49 228 731787; fax: +49 228 735388.
E-mail address: m.famulok@uni-bonn.de (M. Famulok).
† These authors contributed equally to this work.

0968-0896/$ - see front matter © 2013 Elsevier Ltd. All rights reserved.
http://dx.doi.org/10.1016/j.bmc.2013.05.021

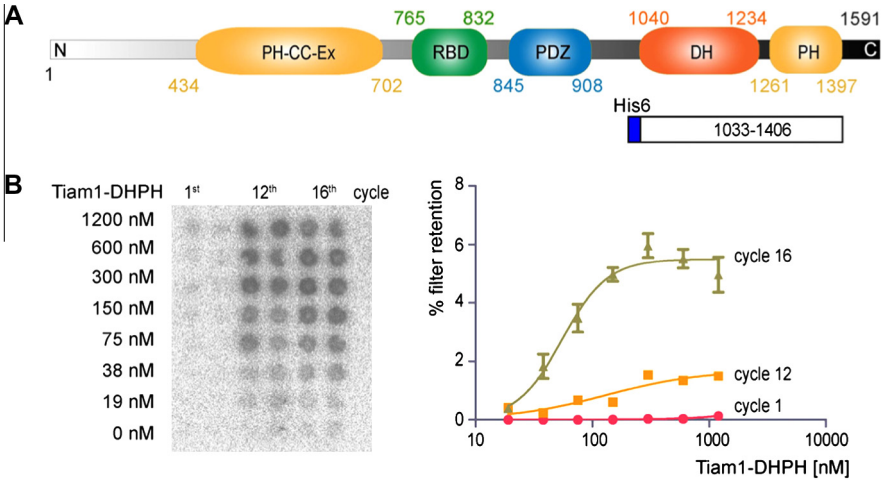

Figure 1. (A) Domain overview of murine Tiam1 with the indicated DHPH construct that has been used in the selection experiment. (B) Filter retention assay of 5′-[^{32}P]-labeled RNA pool after selection round 1, 12 and 16. The quantitative evaluation of the filter retention experiment is shown on the right.

follow an alternative approach directed towards the identification of Tiam1-specific inhibitors, namely the identification of aptamers that bind Tiam1 and interfere with its biological function. Aptamers are nucleic acid-based ligands that have been described as specific binders of a broad variety of different target molecules, and have demonstrated their potential as highly selective, high-affinity protein inhibitors in a variety of studies.[25] Besides their relatively rapid identification in an in vitro process called SELEX (systematic evolution of ligands by exponential enrichment) they often possess inhibitory properties, which make them ideal candidates to modulate protein functions. Interestingly selected aptamers can later be used for a large variety of potential downstream analytical applications like aptamer displacement assays, intracellular studies, sensor applications, as delivery vehicles, for purposes of multiplexing, and many more.[26,27]

The first aptamer that has been reported to target a guanine nucleotide exchange factor was the RNA aptamer M69 that was selected to bind and inhibit the small ArfGEF class of Cytohesins in a pan-selective fashion.[28] Since then, only the aptamer K61 that recognizes Cytohesin-2 has been described.[29] More recently, we found two aptamers called V63 and V88 that specifically targeted various members of the Ras superfamily of small GTPases in a pan-selective fashion, but these aptamers did not interfere with the intrinsic and GEF-mediated guanine nucleotide exchange activities of GTPases.[30]

Here we present the identification and characterization of RNA aptamers that specifically target the DHPH domain of Tiam1, a GEF for the Rho GTPase Rac. Two of these aptamers were found to inhibit the Tiam1 DHPH-mediated activation of Rac in vitro at low micromolar concentration. These new aptamers not only expand the landscape of GEF-specific inhibitors, but may also serve as useful tools for the further elucidation of Tiam1 function in vitro or in cell culture.

2. Results

2.1. In vitro selection

We employed SELEX to isolate RNA aptamers that recognize a domain of the Tiam1 protein that ranges from amino acid residue 1033 to 1406 and comprises of the complete DH domain that harbors the Tiam1 GEF function, and the directly C-terminal following PH domain. This construct also contained a hexahistidine-tag at the N-terminus (Fig. 1A). For immobilization, the Tiam1-DHPH construct was chemically biotinylated by reacting the purified protein with NHS-sulfo-biotin. The resulting purified biotinylated protein was then incubated with Streptavidin coated magnetic Dynabeads, to yield a matrix that was used for the in vitro selection experiment. The RNA library was obtained by in vitro transcription using a PCR-amplified DNA library that comprised a 50 nucleotides random region, flanked by two primer binding sites. The 5′-primer contained the T7 promotor sequence. The resulting RNA library exhibited a complexity of at least 10^{14} different sequences. The RNA library was incubated with the selection matrix and after removal of nonbinding sequences by washing with binding buffer, remaining species were eluted by heating, reverse-transcribed, PCR amplified, and used as input DNA for the next transcription to start a new selection cycle. We performed a total of 16 cycles of selection and amplification. A direct comparison of the unselected pool (Fig. 1B, cycle 1) with the libraries after cycles 12 and 16 for binding to increasing concentrations of Tiam1-DHPH by filter retention revealed no binding for the cycle 1, 2% filter retention for cycle 12, and nearly 6% filter retention for the cycle 16 RNA (Fig. 1B, right panel). This RNA did not bind to Streptavidin beads lacking Tiam1-DHPH. Because the cycle 16 library showed binding saturation at ca. 300 nM protein concentrations without further increase of binding at higher concentrations, the selection was considered to be complete after this cycle.

Sequencing of 33 aptamers revealed 14 different sequences. Among them, clones K60 and K102 occurred twice, and clone K73 three times. The most abundant clone was K11, which appeared sixteen times. The remaining ten other clones represented orphan sequences of which each appeared only once. The complete set of monoclonal aptamer sequences was analyzed with respect to shared sequence motifs. We identified two re-occurring motifs that are shared by many otherwise different sequences. Four clones, K41, K44, K60, and K75 belong to motif 1, which is characterized by a 40 nucleotides long stretch that exhibits a certain degree of sequence homology at individual base positions, and a 15% sequence identity (Fig. 2, upper set of sequences). All other clones belong to the motif 2 class. Motif 2 comprises an AU-rich stretch of 15 nucleotides that share even higher sequence homology at individual positions than motif 1; here the sequence identity was 33%. Motif 2 is particularly rich in conserved adenine residues (Fig. 2, lower set). Based on the observed AU-conservation we consider this motif to represent a consensus sequence.

Clone (frequency)		sequence of randomized region (5' → 3')		K_D
		motif 1		
K60 (2)	UCUGGAGUU	GACGUUGCUUAAGGGCGAAUUCCAGCACACUGGCGGCCG	UU	>1 µM
K75	C	GGAUCGGCAUAAGUAUAAAAUAUAAAUCAACUCCUGCCC	AGAGCUCUA	>1 µM
K44	UUCCAA	UAAAUUCCCUCAGACCCAAUAUGCACUCGCCUUCCACCC	UCUUU	>1 µM
K41	GCC	GUCAUUGCCUAAUUAUAAUAAUUACAACACUUCCUUGUC	CCAUUUGU	>1 µM
		motif 2		
K101		AAUAAUAAUAAAAAC	UCGAUCCUAAAUUACUAUGAUAUUUAUUGAUCCCC	> 1 µM
K43	AACCUGAUAC	AAUAAUAAUAAAAAC	CAUGGAUAAGAACAACCUCUUA	> 1 µM
K73 (3)	AGAUGGUCAU	AAUAAUAAUAAUACC	UUCAACAUAUAAAUUUGUCC	> 1 µM
K9	GCU	AAUAAUAAUAAUAAU	GUAUAUGUAAUUUUUUUCGUGUUGUUGUUUAU	> 1 µM
K102 (2)	CAUAUAUACU	GAACAUAAUAAUAAC	UAAAUUUUUUUACUUUGUC	> 1 µM
K91	CCCCCUG	AAAUAUAAUAAUAAC	UAUGAAUAAUGUAUAAUUGGUAUGCC	<.5 µM
K103	AGAUUACGGA	AAUUAUAAUAACAAU	AAAUAUCCUACUAUUUUCCCCG	< 1 µM
K81	A	AAUAAUAAAAAAUAAU	AAACUUGCCACAUUUCCUUUAAUUAACUUUUCAC	> 1 µM
K87	UACAACAUUU	CAUCAUAAUACCAAG	UUCCCACAUUCGAUAUCG	> 1 µM
K11 (16)	CCCUU	AAUGCUAAUACGACU	CACUAUAGGAAGAAAGAGGUCUGAGACAUU	< 1 µM

Figure 2. Cycle 16 sequences of Tiam1-DHPH-binding RNA aptamers. The sequences that have been cloned from selection cycle 16 are aligned according to the two motifs they belong to. The degree of conservation of individual base positions within each motif is indicated by the height at each position. The numbers in parentheses next to each clone refer to the frequency of occurrence of the respective clone among the 33 sequences. The rough estimation of the dissociation constant is based on one filter binding experiment.

2.2. Determination of binding affinities of selected aptamers

By performing filter retention assays we determined the dissociation constants between individual aptamers and Tiam1. Representative titration curves of the sequences that displayed the highest affinities, namely clones K11, K91, and K103, are shown in Figure 3A. These three members all belong to the motif 2 class. The motif-1-containing aptamers all exhibited lower affinities, as indicated for each clone in Figure 2. Affinity determinations by a filter retention assay revealed that the motif-2-containing sequences displayed higher affinities to Tiam1 than the members of the motif1 class. For the highest affinity binders, clones K11, K91, and K103 we performed a more thorough K_D-determination by performing titrations in filter binding assays using 5′-[^{32}P]-labeled aptamers. To exclude an effect of the 5′-phosphorylation on the affinity we performed a control experiment using the dephosphorylated clones of these aptamers in a competitive filter binding with the radiolabeled sequences.

All non-phosphorylated clones were able to compete with the phosphorylated ones for target binding, indicating that the 5′-phosphorylation had no influence on Tiam1 binding (data not shown). The K_Ds for clones K11, K91, and K103 ranged between 200 and 550 nM (Fig. 3). Among them, clone K91 bound with the highest affinity, displaying a K_D of 200 nM. Expectedly, the binding curves shown in Figure 3A reveal that the monoclonal aptamers all are more efficiently retained on the nitrocellulose membrane by Tiam1-DHPH, as compared with the bulk enriched pools from selection cycle 16.

The secondary structure predictions by lowest energy folding using mfold resulted in different folds for the three highest affinity binders clones K11, K91, and K103 (Fig. 3B). For the mfold calculations, salt and temperature parameters were set to 1 M NaCl and 37 °C. Noticeable is that at least in case of clones K11 and K91 the conserved positions within the motif 2 are all located primarily, if not exclusively, in presumably non-Watson–Crick paired regions in all three secondary structures. Since K91

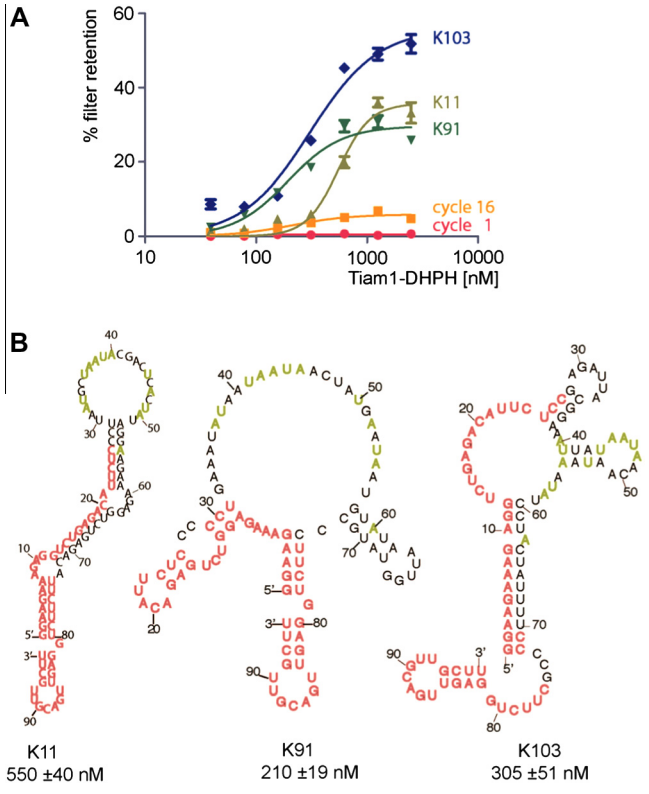

Figure 3. (A) Determination of the dissociation constants of K11, K91 and K103 in filter binding experiments with 5′-[^{32}P]-labeled RNAs. (B) In silico calculation of the lowest energy folding of K11, K91 and K103 using the mfold webserver. Colored in red are constant primer binding sites and all positions that are colored green are conserved positions within the sequence motif 2. Additionally the calculated K_D values from three independent filter-binding experiments are shown.

displayed the highest affinity for Tiam1 it was chosen for further characterization.

2.3. Aptamer K91 selectively binds the Tiam1-DHPH domain

Because the in vitro selection was performed with the DHPH-construct of Tiam1, we next asked whether the aptamer K91 binds specific to the DH-, the PH-, or the DHPH tandem domain of Tiam1. We expressed the respective Tiam1 domains and subjected the purified protein domains to filter retention assays using radiolabeled K91 (Fig. 4A). As evident from Figure 4A, the highest affinity was determined for the DHPH tandem domain of Tiam1. In contrast, the DH domain alone was bound by orders of magnitude weaker; even at 4 μM protein concentration, no saturation of the binding curve was obtained. Basically no binding was observed for the isolated PH domain of Tiam1. This is also true for the unrelated Sec7 domain of the Arf-GEF Cytohesin-2 (ARNO). Because the Sec7 domain was also equipped with the same hexahistidine tag at its N-terminus that was present in the Tiam1-DHPH domain, the lack of binding to His6–Sec7 indicated that the hexahistidine tag does not substantially contribute to the binding to Tiam1-DHPH. We also did not detect any binding of K91 to the closely related DHPH domain of the Rho-GEF Vav1, demonstrating that the recognition of the Tiam1-DHPH domain by K91 occurs with high specificity.

Having shown that the aptamer K91 requires the DHPH tandem domain we next sought to directly compare the binding of K91 to Tiam1-DHPH with binding to the Tiam1-GTPase Rac1, and to the complex between Tiam1 and Rac1. The unselected RNA library B50 was used as a negative control. As evident from Figure 4B, K91 exclusively bound to Tiam1-DHPH, whereas neither Rac1 nor the Tiam1/Rac1-complex were recognized by the aptamer. This result is interesting because it strongly suggests that K91 recognizes a motif on Tiam1 that overlaps with the GTPase binding site. In this case, this binding behavior of K91 might be suited for indirectly narrowing down the binding site of the aptamer on Tiam1.

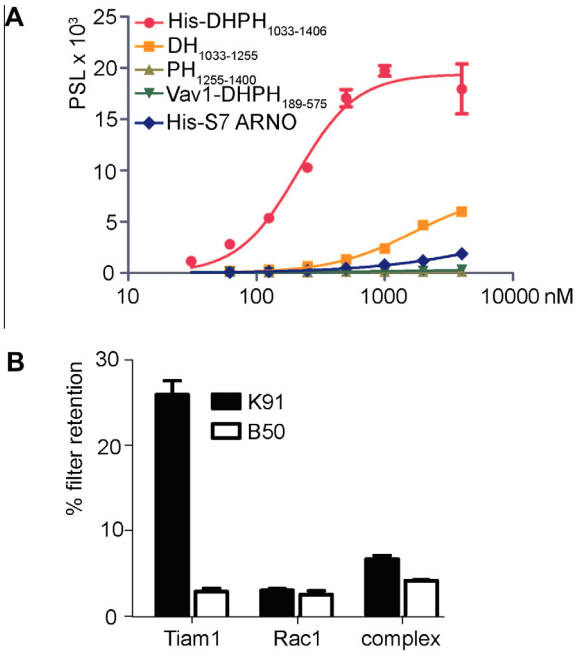

Figure 4. Binding of K91 to individual Tiam1-domains and the Tiam1/Rac1 complex. (A) Filter binding experiment with 5′-[^{32}P]-labeled K91 and different control proteins in order to determine the specificity of K91. (B) Filter binding experiment with 5′-[^{32}P]-labeled K91 and the parent RNA library B50. The RNAs have been incubated with either 1 μM Tiam1, 1 μM of Rac1, or with the pre-assembled complex formed between equimolar amounts of Tiam1 and Rac1 (1 μM).

2.4. Aptamer K91 inhibits Tiam1 GEF activity

Next, the influence of the three selected aptamer clones K11, K91, and K103 on the Tiam1-catalyzed guanine nucleotide exchange on Rac2 was determined. The guanine nucleotide exchange activity of Tiam1 on Rac2 was tested, since the exchange activity on Rac1, the more relevant GTPase substrate, turned out to be too slow in our experiments.[15] We performed the exchange reaction by measuring the association of fluorescent 3′-/2′-methyl anthraniloyl-GDP (mantGDP) to Rac2. The read-out of this assay is based on an increase of mant-fluorescence upon association of mantGDP to its binding site in the protein. The intrinsic rate constant k_{obs} of Rac2 was measured to be 13×10^{-4} s^{-1} (Fig. 5A, black curve). In the presence of Tiam1-DHPH, the k_{obs} raises approximately by sevenfold, namely to 88×10^{-4} s^{-1}(open square curve). As evident from Figure 5A, both K91 and K11 significantly decelerated the Tiam1 catalyzed mantGDP association to Rac2 (K91: dark grey curve; K11: medium grey curve). In contrast, neither the control library B50 nor the aptamer K103 showed a substantial influence on the exchange reaction (Fig. 5A, light grey circle/grey triangle curves). The fact that K103 was inactive as a Tiam1-DHPH inhibitor is interesting in light of its binding constant of 300 nM, which was even lower than that of K11 (550 nM), a clone that did show some inhibitory activity. K91, the aptamer with the high-

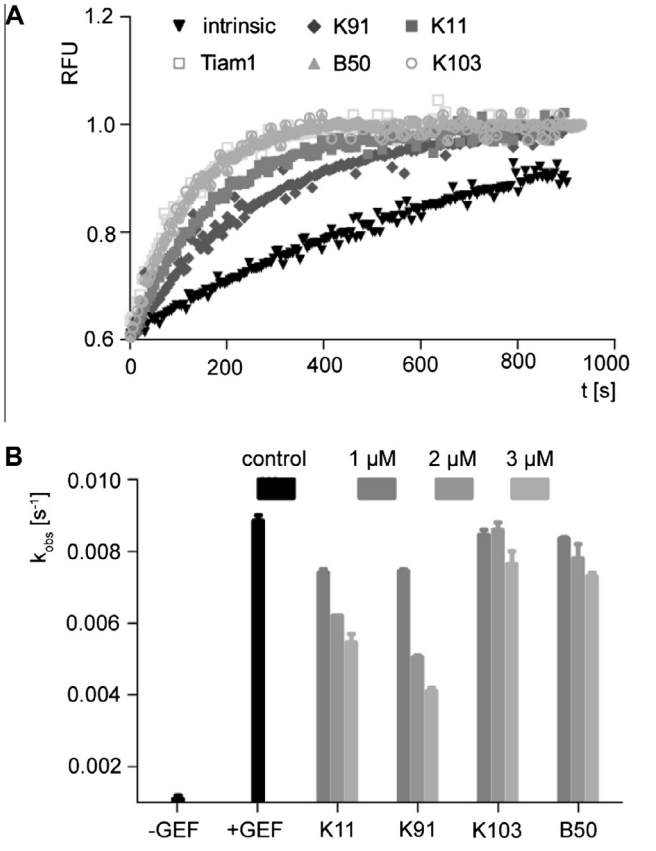

Figure 5. Tiam1-DHPH catalyzed association of mantGDP to Rac2. (A) Kinetic measurement of the Tiam1-catalyzed mantGDP association to Rac2 in presence of aptamers K91 (dark grey rhombi), K11 (medium grey squares), K103 (light grey circles), and the non-binding unselected RNA library B50 (light grey triangles). The K103, and B50 and control without RNA (open squares) curves are overlaid. The intrinsic activity is shown in black. All RNAs were tested at 3 μM. (B) Overview of the mantGDP association experiment for a concentration range of K11, K91, K103 and the B50 RNA library. The reported values of k_{obs} were obtained by at least two independent measurements.

est affinity to Tiam1-DHPH also was the most effective GEF inhibitor. As shown in Figure 5B, the inhibitory activity of aptamers K11 and K91 occurred in a concentration-dependent fashion.

2.5. SHAPE analysis and determination of K91 minimal motif

The full-length sequence of the K91 aptamer comprises of 94 nucleotides, which corresponds to a molecular mass of 31 kDa. For many applications of aptamers, particularly their use in aptamer displacement screens,[31–34] as analytical tools,[35] for structure determinations,[36,37] and for the incorporation of additional functionalities by chemical modifications,[38–41] it is advantageous to identify the minimal motif required for binding and inhibition. In many cases, minimal motifs become immediately apparent from conserved motifs and sequence co-variations,[42–45] or from the in silico-generated secondary structure folding.

We therefore performed selective 2′-hydroxyl acylation analyzed by primer extension-based (SHAPE) probing experiments of the unbound and the Tiam1-DHPH complexed K91 aptamer using *N*-methylisatoic anhydride (NMIA).[46] The chemical probe NMIA is a hydroxyl-selective electrophile that modifies the ribose 2′-OH position at conformationally unconstrained or flexible nucleotides. Figure 6 shows both SHAPE experiments in the absence and presence of Tiam1-DHPH with the graphical evaluation of the normalized SHAPE reactivities for each nucleotide between position 30 and 71 (right upper panel). In addition, the ratios of Tiam1-DHPH bound versus unbound SHAPE reactivities for the corresponding bases are also shown (right lower panel). The region between base positions U31 and G58 is substantially modified by NMIA, interspersed only by two short regions of low reactivity. When Tiam1 is added we have observed altered SHAPE reactivity for U36, A39, U48, A49, A52 and U54 within this region of K91. The SHAPE reactivity of the majority of the other bases in this region does not change much. This finding indicates that Tiam1-DHPH binding may not induce major structural rearrangements within the region between residues 31 and 58. The stem-loop from U59 to G71 clearly agrees with the SHAPE reactivity, particularly position 60–62 and 69 showing reduced signal intensities. After addition of Tiam1-DHPH this motif undergoes a substantial rearrangement, indicated by the drastic change in the reactivity of the majority of the bases within the region between positions 58 and 72.

To substantiate the SHAPE analyses, we devised a series of shortened variants of the full-length aptamer K91. To do so, we also took into account alternative low-energy folds of K91, such as the structure 2 in Figure 7. In this folding, the secondary structure motifs I and III both remain the same as in structure 1 (Fig. 7). However, a new structure motif II appears in which parts of the 3′-primer sequence pair with the long single-stranded region between residues 38 and 53 that contains the conserved sequence motif 2. Motif II consists of a long Watson–Crick-paired helix that also contains two non-canonical base pairs in its middle, namely a CA and an AA, flanked by two GU-wobble pairs on each side.

The first truncated version is based on the folding 1 of K91, in which base positions 79–94 were removed to yield the 78-mer variant **1A**. This variant not only bound to Tiam1-DHPH with a K_D of 280 nM, but also inhibited Tiam1 GEF activity on Rac2, similar to the full-length K91 aptamer (Table 1). The next truncated construct was variant **2A** that is rationalized based on the folding shown in structure 2. We deleted the entire motif III and closed the remaining helix motif II with a stable GNRA-loop, leaving a total of 66 nucleotides in this variant. As summarized in Table 1, variant **2A** exhibited similar affinity for Tiam1-DHPH as **1A** or K91 (250 nM). Strikingly, however, despite its high-affinity binding, the truncation in **2A** resulted in a complete loss of inhibition of the Tiam1-catalyzed GDP/GTP exchange on Rac2. In construct **2B** we deleted motif I that comprises the entire 5′-primer region, including the presumably single-stranded nucleotides 32–37. This 54-mer variant retained some affinity to Tiam1-DHPH, but with a value of 850 nM the K_D of variant **2B** was approximately fourfold reduced as compared to the full-length K91 sequence. Again, this truncated variant did not inhibit the Tiam1-catalyzed GDP/GTP exchange on Rac2 (Table 1). Finally, we further shortened **2B** by removing three more base pairs at the terminus of the proposed helical region of motif II. The resulting truncated construct **2C** was 48 nucleotides in length. As evident from the data in Table 1, **2C** completely lost its affinity for the Tiam1-DHPH domain and did not show any inhibition in the GDP/GTP exchange assay.

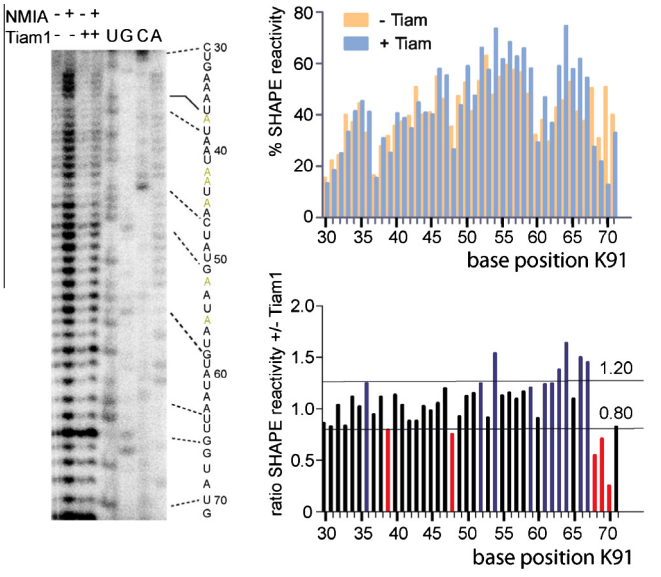

Figure 6. SHAPE analysis of K91 in the absence and presence of Tiam1-DHPH. SHAPE analysis sequencing gel with appended sequencing ladder. The normalized reactivities for both reactions in the presence and absence of Tiam1-DHPH were plotted in the upper graph on the right. The graph below shows the SHAPE reactivity ratios +/− Tiam1-DHPH. Bars in red indicate reduced reactivity of at least 20%, blue bars indicate increased reactivity of at least 20%.

3. Discussion

The interaction of Tiam1 with its main target Rac1, a Rho GTPase, is characterized by the loss of more than 2800 Å^2 of solvent accessible area on both Tiam1 and Rac1.[47] The surface that gets restructured after complex formation is a potential point of action for small molecule inhibitors. However, targeting protein–protein interactions that span over such large areas is rather difficult when using low molecular weight compounds, given the fact that often both surfaces are flat without deep grooves or clefts.[48] Taking this into consideration, we performed SELEX to identify aptamers that inhibit the GEF function of Tiam1.

The three related Tiam1-binding RNA-aptamer sequences that we found exhibit similar affinities in the upper nanomolar range, but only two of them, clones K11 and K91 also inhibited the GEF activity of Tiam1. Based on their primary sequences, an intuitive explanation of the lack of inhibition by clone K103 is difficult, the more so, as all three sequences share a common motif that consists of a 15 nucleotides long AU-stretch. However, according to the in silico calculations of their secondary structures, and confirmed by the SHAPE probing data that we performed with clone K91, there are some differences in the folding context in which the conserved regions reside. In case of both K11 and K91, the motif resides almost entirely within a longer unpaired region, flanked by Watson–Crick-paired helices. In case of K103, the folding context is somewhat different, as the conserved motif may be part of

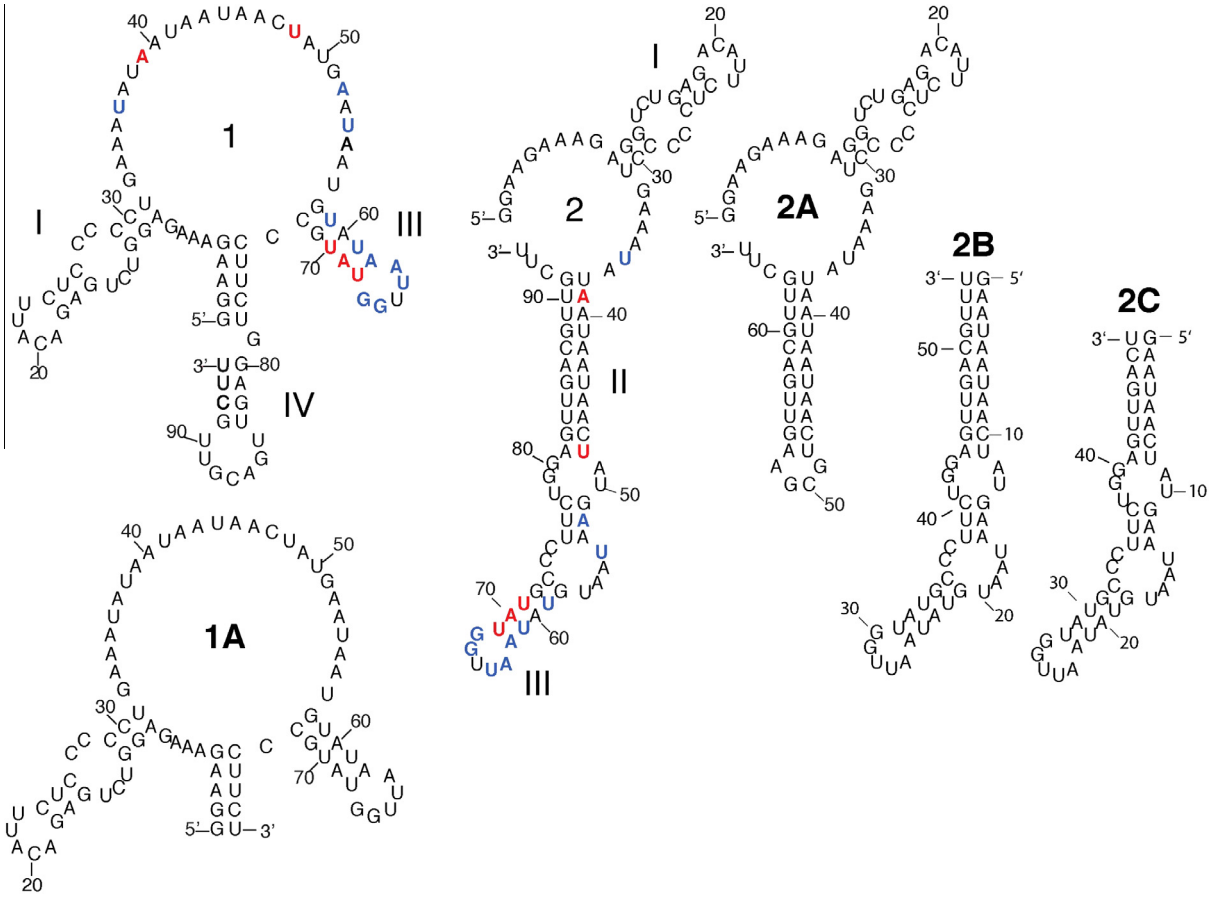

Figure 7. Two alternative secondary structure folds of aptamer K91 based on potential in silico low-energy foldings, SHAPE data, and truncated variants of K91. Roman numerals refer to individual sequence motifs within each secondary structure. The colored base positions refer to the SHAPE data shown in Figure 6. The truncated variants of K91 used in this study are indicated in bold.

Table 1
Affinity and inhibition of shortened K91 constructs

K91 variant	K_D [nM]	Inhibition of Tiam1 GEF activity[a]
K91 full-length	209 ± 45	++
1A	280 ± 60	++
2A	255 ± 45	–
2B	850 ± 150	–
2C	No binding	–

[a] Measured by mantGDP exchange on Rac2.

a short helix. Our data indicate that the conserved motif is important for aptamer function, but whether it is essential for binding, or for inhibition, or both, cannot be reliably deduced from our data.

The recognition of the isolated DH domain of Tiam1 by the aptamer K91 is substantially worse than that of the entire DHPH domain. The same is true for the isolated PH domain. This means that either the PH domain is providing additional binding sites to achieve high-affinity binding, or that the PH domain is important for stabilizing the conformation of the whole DHPH construct. The latter assumption is plausible, since the neighboring PH domain is known to stabilize the helix α9 that connects the DH with the PH domain (Fig. 8).[47] Conversely, in the isolated DH domain the C-terminus likely exhibits considerably higher flexibility, and this reduced conformational integrity might impair the binding of the aptamer. Also, K91 does not recognize the related DHPH-CRD domain of Vav1. This finding suggests that the aptamer binds at least partially outside the conserved regions of the DH domain. Based on these observations, we hypothesize that the helix α9 might

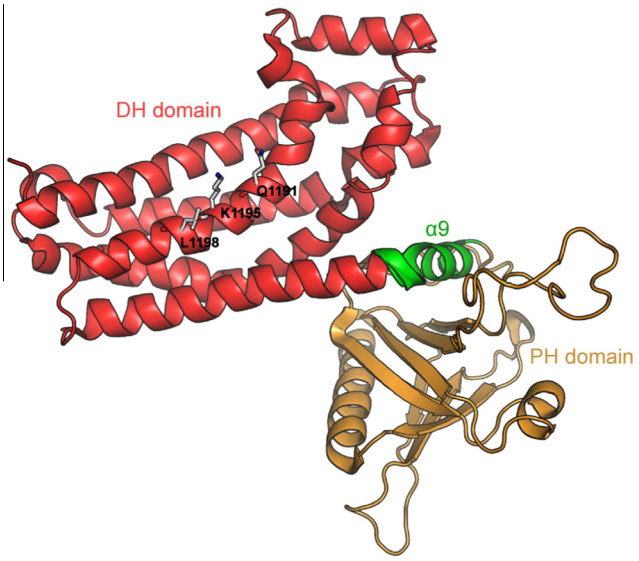

Figure 8. Tiam1-DHPH domain based on the pdb entry 1FOE with the indicated DH domain in red, the PH domain in bright orange, the α9 helix in green and shown as stick representation are the residues Q1191, K1195 and L1198.

constitute an important recognition site of the aptamer. Comparing the sequence of the α9 helix of Tiam1-DHPH (aa 1239–1249, pdb 1FOE)[47] with the corresponding helix in the Vav1 crystal structure (aa 379–389, pdb 3FJI)[49] there are no apparent sequence

similarities detectable. These data suggest that helix α9 of Tiam1-DHPH might be involved as a binding element for K91 and possibly to also account for the specificity. Additionally, the filter retention assays that we have performed with the Tiam1/Rac1 complex clearly revealed a strong decrease in binding after Rac1 has been added. The binary GEF/GTPase complex is likely to be stably formed under these assay conditions. Previous studies have shown that the ternary GEF/GTPase/nucleotide complex is less stable than the binary GEF/GTPase complex.[50,51] Thus, the aptamer binding site might overlap with residues that are important for GTPase complexation. Again, this notion is in accordance with data derived from the co-crystal of Tiam1-DHPH with Rac1, where Rac1 forms contacts not only with the CR1 and CR3 region but also with the C-terminal part of helix α9. However, we cannot exclude the possibility that Rac1 induces conformational changes on Tiam1 that prevent the aptamer from binding to the protein.

On the basis of mfold calculations and SHAPE probing experiments we shortened K91 in order to derive structural elements that are potentially important for binding and inhibition of Tiam1-DHPH (Fig. 7). Stem motifs I and III are indispensable for the inhibition of the GEF activity of Tiam1 and particularly motif III undergoes a substantial rearrangement after Tiam1 binding. Surprisingly, both motifs I and III do not seem to be major recognition elements involved in binding Tiam1, since their deletion is not accompanied by a significant loss in affinity (Table 1). Based on our data we hypothesize that the major binding element of K91 may either reside within structural motif II or within the unpaired region from position A37 to U48. The extension of this binding element by motifs I and/or III is required for the aptamer to achieve inhibition of the GEF-activity.

In summary, we propose that helix α9 of Tiam1 comprises an important recognition element for K91. With respect to the aptamer, the structural motif II likely contains the Tiam1-DHPH binding motif, whereas the inhibition of the GEF activity by motifs I and III, presumably occurs by sterical interference with the residues Q1191, K1195, and L1198 that are located within the CR3 region of Tiam1 and are essential for the GEF activity (Fig. 8). Through the selection of the specific and inhibitory RNA aptamer K91, we have addressed protein surface areas of the DHPH tandem domain that potentially serve as target sites for small molecule inhibitors. Due to its strong specificity over the closely related GEF Vav1, K91 might be a promising tool for further elucidation of the ambiguous biological roles of Tiam1.

4. Experimental

4.1. Protein expression

The expression plasmid pPROExHtb of Tiam1 (aa 1033–1406, mouse) was kindly provided by Prof. John Sondek (UC Chapel Hill, North Carolina, USA). The isolated DH and PH domains of Tiam1 were PCR-amplified from pPROExHtb Tiam1 (aa 1033–1406). Tiam1 (1033–1255, DH) was subcloned into a pET SUMO vector and Tiam1 (aa 1255–1400, PH) was subcloned (BamHI, EcoRI) into a pGEX2T modified with a TEV-recognition sequence. Vav1 (aa 189–575, human) was subcloned via BamHI, EcoRI into a modified pGEX2T and additionally mutated at aa 351 (M351T) to increase solubility in *Escherichia coli*. Rac2 (aa 1–192, human) was subcloned into a pET SUMO vector. Rac1 (aa 1–192, human) was sublconed via BamHI/EcoRI into a pGEX2T vector modified with a TEV-recognition sequence. Tiam1 (DH-PH), Tiam1 (DH), Rac2, Arf1 (NΔ17) and the Sec7 domain of Cytohesin-2 (ARNO) were expressed with N-terminal His6-tags and subsequently purified on Ni-NTA agarose (Machery Nagel, Hilden, Germany). Tiam1 (PH) Vav1 (DH-PH-CRD) and Rac1 were expressed with an N-terminal GST-tag and accordingly purified on GSH agarose (Protino, Machery Nagel, Hilden, Germany) before the incubation with TEV protease to remove the GST tag

4.2. Biotinylation of Tiam1-DHPH

Tiam1-DHPH was first brought into 1× PBS buffer, concentrated to 1 mg/ml and thereafter incubated with a 2- to 3-fold molar excess of freshly dissolved NHS-Sulfo-Biotin (Pierce protein science) in 1× PBS buffer. The reaction was terminated after 1 h at room temperature with excess Tris buffer. Unreacted NHS-Sulfo-Biotin was removed by running a desalting column on an Äkta FPLC (GE Healthcare). In order to verify the coupling 1–3 μl of biotinylated Tiam1 and non-biotinylated control protein was spotted on a nitrocellulose membrane, allowed to dry and after repetitive washing steps with 1× PBS buffer incubated with an anti-Biotin-FITC labeled-antibody (BN-34, Sigma–Aldrich) for 40 min at room temperature under subdued light conditions. Eventually the biotinylation was visualized on a fluorescent image analyzer (FujiFilm, FLA-3000).

4.3. Preparation of affinity resin

500 μl of Streptavidin coated Dynabeads (Dynabeads M-280, Life Technologies) were sequentially washed 2× with 500 μl [1× PBS/1 mM $MgCl_2$ |1× PBS/1 mM $MgCl_2$/1 mg/ml BSA |1× PBS/1 mM $MgCl_2$] before the incubation with 100 μg (2.2 nmol) biotinylated Tiam1-DHPH for 30 min at 22 °C in an overhead tumbler. Thereafter the beads were washed 2× with 500 μl [1× PBS/1 mM $MgCl_2$/1 mg/ml BSA |1× PBS/1 mM $MgCl_2$], respectively. The beads were finally brought into 1500 μl of 1× PBS/1 mM $MgCl_2$/1 mg/ml BSA and stored at 4 °C for the entire selection process.

4.4. In vitro selection

The DNA library 5′-AAT GCT AAT ACG ACT CAC TAT AGG AAG AAA GAG GTC TGA GAC ATT GA-N50-GAA GAC CTC AAC TGC AAC GAA-3′ (N50: 50 bases randomized) was PCR amplified using the following oligodeoxynucleotides: 5′-AAT GCT AAT ACG ACT CAC TAT AGG AAGAAAGAGGTCTGAGACATT-3′ and 5′-AAGCAACGT-CAACTCCAGAAG-3′. PAGE purified RNA transcripts were dissolved in selection buffer (1× PBS, 1 mM $MgCl_2$, pH 7.4) and incubated with Streptavidin coated Dynabeads that have been loaded with biotinylated-His_6-Tiam1 (DHPH) for 30 min at 37 °C. Unbound RNAs were washed away with selection buffer using a magnetic holder, and bound RNAs were heat-eluted at 80 °C for 5 min. Eluted RNA was reverse transcribed, PCR-amplified and finally in vitro transcribed. For the first selection round 5 nmol RNA (sequence diversity: 4×10^{14} sequences) has been used. The in vitro selection scheme was repeated for 16 cycles, thereafter TOPO-TA cloned, transformed into *E. coli* and individual clones sequenced (GATC Biotech, Konstanz, Germany).

4.5. Filter retention assay

5–10 nM of [^{32}P] end-labeled RNA was incubated in 1× PBS/1 mM $MgCl_2$ with increasing concentrations of the respective proteins in a total volume of 25 μl. After an incubation period of 30 min at 23 °C the RNA/protein complex was vacuum filtered through a moistened nitro cellulose membrane and washed with a total volume of 1 ml 1× PBS/1 mM $MgCl_2$. The membrane was transferred to a cassette and exposed to a phosphorimager screen overnight and quantified the next day on the phosphorimager (Fujifilm BAS-2500).

4.6. In silico prediction of RNA folding

The RNA sequences of K11, K91 and K103 have been analyzed with the mfold program package that is available on the internet: http://mfold.rna.albany.edu.

4.7. Guanine nucleotide exchange assay

The GTPase Rac2 (final 2 μM) was incubated in guanine nucleotide exchange buffer (1× PBS/5 mM $MgCl_2$) with 200 nM Tiam1 (DHPH) and the corresponding RNA for 10 min at 23 °C in a total volume of 950 μl in a quartz glass cuvette. After the incubation the exchange reaction was initiated by injecting 50 μl of a 8 μM mantGDP (Jena Biosciences, Germany) solution. The fluorescence was read in 10 s intervals at 360/440 nm for 1800 s on a fluorescence spectrometer (Perkin Elmer, LS 55, Fluorescence spectrometer).

4.8. SHAPE analysis

5 pmol of K91 were heated for 2 min at 95 °C in 0.5× TE buffer and immediately cooled down on ice for 2 min before the addition of folding buffer (final: 1× PBS, 3 mM $MgCl_2$). Then either Tiam1 (final: 5 μM) or buffer was added and incubated for 20 min at 22 °C. 5 min prior to the probing reaction, 5.4 mg *N*-methylisatoic anhydride (Sigma) was dissolved in 508 μl 100% DMSO to get a 60 mM solution and further diluted with an equal volume of water to 30 mM in 50% DMSO. Subsequently, the freshly prepared NMIA solution was added to a final concentration of 3 mM (5% DMSO). The reaction was allowed to proceed for 1 h and 35 min (estimated 2.5 hydrolysis half-lives). The reaction was terminated with NaOAc/EtOH precipitation of K91. The RNA pellet was redissolved in 10 μl 0.5× TE buffer and further processed in a primer extension reaction using AMV Reverse Transcriptase (Promega) and 5′-[^{32}P]-labeled reverse primer. After precipitation of the product the DNA was resuspended in PAGE loading buffer and loaded on a 10% Sequencing PAGE gel. The gel was quantified on a Fujifilm FLA-3000 Phosphorimager using the AIDA software package. For each base the signal of the −NMIA reaction was subtracted from the corresponding +NMIA sample and divided by the total counts of both to give the % SHAPE reactivity value. The total number of counts for all +Tiam1 and −Tiam1 reactions were normalized to approximately 100,000 counts (PSL).

4.9. Sequencing reaction

The reference sequencing ladder of K91 was generated according to the manufacturers' protocol (Sequenase Sequencing Kit, Affymetrix).

Acknowledgments

This work was supported by the Deutsche Forschungsgemeinschaft, the SFB 704, and the NRW Forschungsschule LIMES Chemical Biology. We thank Nicole Krämer for help in performing SHAPE experiments, G. Mayer and A. Itzen for valuable discussions, and G. Bendas for help with fluorescence spectrometry.

References and notes

1. Vigil, D.; Cherfils, J.; Rossman, K. L.; Der, C. J. *Nat. Rev. Cancer* **2010**, *10*, 842.
2. Hall, A. *Science* **1998**, *279*, 509.
3. Ridley, A. J. *J. Cell Sci.* **2001**, *114*, 2713.
4. Sahai, E.; Marshall, C. J. *Nat. Rev. Cancer* **2002**, *2*, 133.
5. Eva, A.; Aaronson, S. A. *Nature* **1985**, *316*, 273.
6. Whitehead, I. P.; Khosravi-Far, R.; Kirk, H.; Trigo-Gonzalez, G.; Der, C. J.; Kay, R. *J. Biol. Chem.* **1996**, *271*, 18643.
7. Chan, A. M.; Takai, S.; Yamada, K.; Miki, T. *Oncogene* **1996**, *12*, 1259.
8. Whitehead, I.; Kirk, H.; Kay, R. *Oncogene* **1995**, *10*, 713.
9. Whitehead, I.; Kirk, H.; Tognon, C.; Trigo-Gonzalez, G.; Kay, R. *J. Biol. Chem.* **1995**, *270*, 18388.
10. Horii, Y.; Beeler, J. F.; Sakaguchi, K.; Tachibana, M.; Miki, T. *EMBO J.* **1994**, *13*, 4776.
11. Chan, A. M.; McGovern, E. S.; Catalano, G.; Fleming, T. P.; Miki, T. *Oncogene* **1994**, *9*, 1057.
12. Katzav, S.; Martin-Zanca, D.; Barbacid, M. *EMBO J.* **1989**, *8*, 2283.
13. Habets, G. G.; Scholtes, E. H.; Zuydgeest, D.; van der Kammen, R. A.; Stam, J. C.; Berns, A.; Collard, J. G. *Cell* **1994**, *77*, 537.
14. Michiels, F.; Habets, G. G.; Stam, J. C.; van der Kammen, R. A.; Collard, J. G. *Nature* **1995**, *375*, 338.
15. Haeusler, L. C.; Hemsath, L.; Fiegen, D.; Blumenstein, L.; Herbrand, U.; Stege, P.; Dvorsky, R.; Ahmadian, M. R. *Methods Enzymol.* **2006**, *406*, 1.
16. Malliri, A.; van der Kammen, R. A.; Clark, K.; van der Valk, M.; Michiels, F.; Collard, J. G. *Nature* **2002**, *417*, 867.
17. Walch, A.; Seidl, S.; Hermannstadter, C.; Rauser, S.; Deplazes, J.; Langer, R.; von Weyhern, C. H.; Sarbia, M.; Busch, R.; Feith, M.; Gillen, S.; Hofler, H.; Luber, B. *Mod. Pathol.* **2008**, *21*, 544.
18. Engers, R.; Mueller, M.; Walter, A.; Collard, J. G.; Willers, R.; Gabbert, H. E. *Br. J. Cancer* **2006**, *95*, 1081.
19. Minard, M. E.; Herynk, M. H.; Collard, J. G.; Gallick, G. E. *Oncogene* **2005**, *24*, 2568.
20. Hordijk, P. L.; ten Klooster, J. P.; van der Kammen, R. A.; Michiels, F.; Oomen, L. C.; Collard, J. G. *Science* **1997**, *278*, 1464.
21. Uhlenbrock, K.; Eberth, A.; Herbrand, U.; Daryab, N.; Stege, P.; Meier, F.; Friedl, P.; Collard, J. G.; Ahmadian, M. R. *J. Cell Sci.* **2004**, *117*, 4863.
22. Bouquier, N.; Vignal, E.; Charrasse, S.; Weill, M.; Schmidt, S.; Leonetti, J. P.; Blangy, A.; Fort, P. *Chem. Biol.* **2009**, *16*, 657.
23. Blangy, A.; Bouquier, N.; Gauthier-Rouviere, C.; Schmidt, S.; Debant, A.; Leonetti, J. P.; Fort, P. *Biol. Eur. Cell Biol. Org.* **2006**, *98*, 511.
24. Schmidt, S.; Diriong, S.; Mery, J.; Fabbrizio, E.; Debant, A. *FEBS Lett.* **2002**, *523*, 35.
25. Bouquier, N.; Fromont, S.; Zeeh, J. C.; Auziol, C.; Larrousse, P.; Robert, B.; Zeghouf, M.; Cherfils, J.; Debant, A.; Schmidt, S.; Mayer, G. *Angew. Chem., Int. Ed.* **2009**, *48*, 2672.
26. Niebel, B.; Lentz, C.; Pofahl, M.; Mayer, G.; Hoerauf, A.; Pfarr, K. M.; Famulok, M. *Chemistry* **2010**, *16*, 11100.
27. Rohrbach, F.; Karadeniz, H.; Erdem, A.; Famulok, M.; Mayer, G. *Anal. Biochem.* **2012**, *421*, 454.
28. Mayer, G.; Blind, M.; Nagel, W.; Bohm, T.; Knorr, T.; Jackson, C. L.; Kolanus, W.; Famulok, M. *Proc. Natl. Acad. Sci. U.S.A.* **2001**, *98*, 4961.
29. Theis, M. G.; Knorre, A.; Kellersch, B.; Moelleken, J.; Wieland, F.; Kolanus, W.; Famulok, M. *Proc. Natl. Acad. Sci. U.S.A.* **2004**, *101*, 11221.
30. Hons, M.; Niebel, B.; Karnowski, N.; Weiche, B.; Famulok, M. *ChemBioChem* **2012**, *13*, 1433.
31. Famulok, M. *J. Med. Chem.* **2009**, *52*, 6951.
32. Hafner, M.; Schmitz, A.; Grune, I.; Srivatsan, S. G.; Paul, B.; Kolanus, W.; Quast, T.; Kremmer, E.; Bauer, I.; Famulok, M. *Nature* **2006**, *444*, 941.
33. Hafner, M.; Vianini, E.; Albertoni, B.; Marchetti, L.; Grüne, I.; Gloeckner, C.; Famulok, M. *Nat. Protoc.* **2008**, *3*, 579.
34. Yamazaki, S.; Tan, L.; Mayer, G.; Hartig, J. S.; Song, J. N.; Reuter, S.; Restle, T.; Laufer, S. D.; Grohmann, D.; Kräusslich, H. G.; Bajorath, J.; Famulok, M. *Chem. Biol.* **2007**, *14*, 804.
35. Famulok, M.; Mayer, G. *Acc. Chem. Res.* **2011**, *44*, 1349.
36. Kettenberger, H.; Eisenführ, A.; Brueckner, F.; Theis, M.; Famulok, M.; Cramer, P. *Nat. Struct. Mol. Biol.* **2006**, *13*, 44.
37. Yang, Y.; Kochoyan, M.; Burgstaller, P.; Westhof, E.; Famulok, M. *Science* **1996**, *272*, 1343.
38. Jäger, S.; Famulok, M. *Angew. Chem., Int. Ed.* **2004**, *43*, 3337.
39. Jäger, S.; Rasched, G.; Kornreich-Leshem, H.; Engeser, M.; Thum, O.; Famulok, M. *J. Am. Chem. Soc.* **2005**, *127*, 15071.
40. Thum, O.; Jäger, S.; Famulok, M. *Angew. Chem., Int. Ed.* **2001**, *40*, 3990.
41. Vinkenborg, J. L.; Mayer, G.; Famulok, M. *Angew. Chem., Int. Ed.* **2012**, *51*, 9176.
42. Burgstaller, P.; Famulok, M. *Angew. Chem., Int. Ed.* **1994**, *33*, 1084.
43. Burgstaller, P.; Kochoyan, M.; Famulok, M. *Nucleic Acids Res.* **1995**, *23*, 4769.
44. Famulok, M. *J. Am. Chem. Soc.* **1994**, *116*, 1698.
45. Famulok, M.; Hüttenhofer, A. *Biochemistry* **1996**, *35*, 4265.
46. Merino, E. J.; Wilkinson, K. A.; Coughlan, J. L.; Weeks, K. M. *J. Am. Chem. Soc.* **2005**, *127*, 4223.
47. Worthylake, D. K.; Rossman, K. L.; Sondek, J. *Nature* **2000**, *408*, 682.
48. Whitty, A.; Kumaravel, G. *Nat. Chem. Biol.* **2006**, *2*, 112.
49. Chrencik, J. E.; Brooun, A.; Zhang, H.; Mathews, II; Hura, G. L.; Foster, S. A.; Perry, J. J.; Streiff, M.; Ramage, P.; Widmer, H.; Bokoch, G. M.; Tainer, J.; Weckbecker, G.; Kuhn, P. *J. Mol. Biol.* **2008**, *380*, 828.
50. Klebe, C.; Prinz, H.; Wittinghofer, A.; Goody, R. S. *Biochemistry* **1995**, *34*, 12543.
51. Lenzen, C.; Cool, R. H.; Prinz, H.; Kuhlmann, J.; Wittinghofer, A. *Biochemistry* **1998**, *37*, 7420.